Received: 1 January 2023 | Revised: 20 February 2023 | Accepted: 1 March 2023

DOI: 10.1002/smm2.1208

RESEARCH ARTICLE

SmartMat Open Access WILEY

Enabling rechargeable Li-MnO_2 batteries using ether electrolytes

Dawei Xia[1] | **Hongpeng Gao**[2] | **Mingqian Li**[3] | **John Holoubek**[1] | **Qizhang Yan**[2] | **Yijie Yin**[2] | **Panpan Xu**[1] | **Zheng Chen**[1,2,3,4]

[1]Department of NanoEngineering, University of California San Diego, La Jolla, California, USA

[2]Program of Materials Science and Engineering, University of California San Diego, La Jolla, California, USA

[3]Program of Chemical Engineering, University of California San Diego, La Jolla, California, USA

[4]Sustainable Power and Energy Center, University of California San Diego, La Jolla, California, USA

Correspondence
Zheng Chen, Department of NanoEngineering, University of California San Diego, La Jolla, CA 92093, USA.
Email: zhengchen@eng.ucsd.edu

Funding information
National Science Foundation, Grant/Award Numbers: DMR-2011924, ECCS-1542148

Abstract

A low-carbon future demands more affordable batteries utilizing abundant elements with sustainable end-of-life battery management. Despite the economic and environmental advantages of Li-MnO_2 batteries, their application so far has been largely constrained to primary batteries. Here, we demonstrate that one of the major limiting factors preventing the stable cycling of Li-MnO_2 batteries, Mn dissolution, can be effectively mitigated by employing a common ether electrolyte, 1 mol/L lithium bis(trifluoromethanesulfonyl)imide (LiTFSI) in 1,3-dioxane (DOL)/1,2-dimethoxyethane (DME). We discover that the suppression of this dissolution enables highly reversible cycling of the MnO_2 cathode regardless of the synthesized phase and morphology. Moreover, we find that both the $LiPF_6$ salt and carbonate solvents present in conventional electrolytes are responsible for previous cycling challenges. The ether electrolyte, paired with MnO_2 cathodes is able to demonstrate stable cycling performance at various rates, even at elevated temperature such as 60°C. Our discovery not only represents a defining step in Li-MnO_2 batteries with extended life but provides design criteria of electrolytes for vast manganese-based cathodes in rechargeable batteries.

KEYWORDS

ether-based electrolytes, Li-MnO_2 batteries, Mn deposition, Mn dissolution, reuse of primary batteries

1 | INTRODUCTION

The lithium-ion battery (LIB) has become an indispensable energy storage solution. However, it is still challenging to balance the cost, sustainability, and performance, where the cathode is often considered as the bottleneck.[1] To enable the long-term deployment of LIBs at scale, reducing and eliminating Ni and Co in cathodes is crucial due to the cost and supply chain issues associated with their limited and geographically concentrated supply.[2] Generally, applying earth-abundant materials, such as Fe or Mn, in said cathodes has the potential to overcome these materials supply challenges. Among the materials utilizing these elements, MnO_2 has one of the deepest histories of application as an electrode material, dating back to 1866.[3] In addition to its economic and

environmental advantages, the high theoretical specific capacity (308 mAh/g, based on one-electron reaction), diverse polymorphs and chemical tunability make MnO_2 particularly desirable. Endowed by these merits, MnO_2 was commercialized as primary batteries utilizing electrolytic manganese dioxide (EMD) cathodes in the 1970s, which are now consumed at scales in the hundreds of millions of cells.[4] However, the commercial success of rechargeable MnO_2 cells remains limited due to issues associated with their cyclability.

Historically, MnO_2, (i.e., pyrolusite MnO_2) was explored in secondary batteries to explore the benefits of nanostructures in the 2000s. Before that, this phase was recognized as electrochemically inactive in the bulk form, due to its sluggish lithium diffusion and rapid irreversible transformation to spinel $LiMn_2O_4$ (LMO).[5] However, despite the impact of such nanostructures, the reported cycling stability of such materials remained untenable for commercial means. This behavior is thought to be largely a result of proton exposure, including the hydrolysis of PF_6^- and solvent (ethylene carbonate, EC) deprotonation at the cathode/electrolyte interface.[6] For example, Bruce et al. reported mesoporous β-MnO_2 of 10 nm wall thickness delivered a first cycle capacity of 292 mAh/g while only 50 charge/discharge cycles (53% capacity retention) were reported.[7] Though MnO_2 is known to suffer acutely from these concerns, such degradation is broadly observed in Mn-based cathodes. For example, it is a consensus that LMO suffers from unwanted Mn^{2+} dissolution and performance decay in carbonate-based electrolytes.[8] Acid species generated in commercial carbonate electrolytes can accelerate the disproportionation reaction of Mn^{3+}, forming soluble Mn^{2+}. Different strategies have been implemented to stabilize cathode/electrolyte interface to reduce such dissolution, including surface coating, doping, electrolytes additives, and functionalized binders.[9] However, fundamentally suppressing Mn dissolution in sustainable Mn-based cathodes remains a grand challenge.[8]

It is proposed that electrolyte redesign is a promising approach to minimize Mn dissolution. Ideally, the electrolytes should be acid-free during storage and electrochemical cycling. Thus, ether-electrolytes utilizing lithium imide salts with limited tendency of hydrolysis become candidates. The other enlightening fact is that the operation voltage of MnO_2 is below 4 V (vs. Li^+/Li), which well matches the stability window of ether solvents. Our rationale for paring MnO_2 cathode and ether electrolytes as more sustainable cell chemistry is presented in Schematic 1.

Herein, we report that the application of an ordinary ether electrolyte (1 mol/L LiTFSI DOL/DME 50/50 in volume) in MnO_2 secondary cells vastly improves cycling performance via the suppression of Mn dissolution. We find that this stabilization is both a function of replacement of $LiPF_6$ in the electrolyte with LiTFSI, and the replacement of carbonate solvents with ether solvents. Application of this ether electrolyte was found to provide > 90% capacity retention over 200 cycles in a wide variety of MnO_2 polymorphs in both nano-scale and micron-scale morphologies, indicative of the versatility of this strategy. While X-ray adsorption near edge spectroscopy (XANES) spectra shows direct evidence of Mn^{3+} in cycled MnO_2, Mn dissolution is minimized in the ether system. This study not only offers a new strategy to enable the reversible cycling of Li-MnO_2 batteries, but also enlightens further examination of the role of electrolyte chemistry in the long-term stabilization of Mn-based cathodes.

2 | RESULTS AND DISCUSSIONS

Though many MnO_2 polymorphs have been reported, β-MnO_2 was initially chosen as a model material for its one-phase reaction mechanism (after initial cycles) at the nanoscale offering desirable structural integrity.[7a] More importantly, the phase with tunnel homogeneity (1 × 1) is free of guest ions, including protons that are

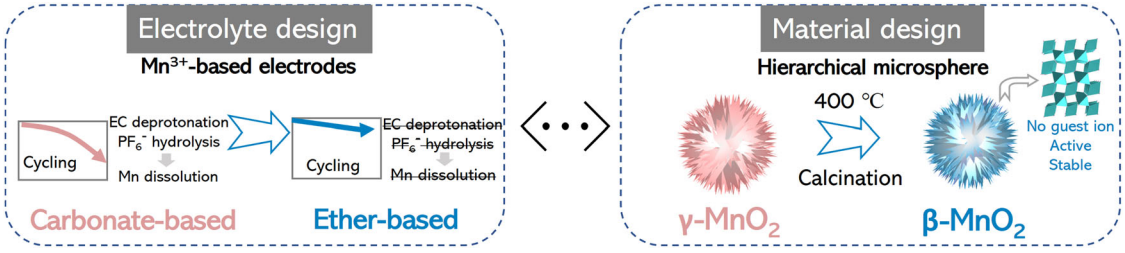

SCHEME 1 The left panel demonstrates the strategy to eliminate protonic species in battery cycling for minimizing Mn dissolution. The right panel exhibits the synthetic route of hierarchical β-MnO_2 microsphere. Such a model MnO_2 cathode offers a platform for electrolyte comparison.

potentially detrimental to interfacial stability of cathodes.[10] In this work, a unique nanotubes-assembled hierarchical β-MnO_2 microsphere (denoted as h-β-MnO_2) was designed by a rapid thermal treatment (400°C, 4 h) from γ-MnO_2 as depicted in Schematic 1. Upon heating, structural water was continuously removed until above 300°C, shown by thermogravimetric analysis (TGA) in Figure 1A. The removal of crystalline water inside the tunnel structure was observed along with the shrinkage of the lattice parameter (Figure S1A). The subsequent γ-β phase transition (Figure S1B) occurred between 350°C and 400°C, is in good agreement with previous work.[11] As shown in Figure 1B, the h-β-MnO_2 of tetragonal rutile structure was identified as space group $P4_2/mnm$. The material presents a Brunauer–Emmett–Teller (BET) specific surface area of approximately 27 m^2/g with limited mesopores (Figure 1C).

To examine the structure properties, electron microscopic imaging including scanning electron microscope (SEM) and transmission electron microscopy (TEM) were performed. From the SEM images (Figure 1D), the h-β-MnO_2 presents particle sizes between 2 μm and 4 μm with a densely packed structure suggested by low-magnification TEM images. The secondary structure is composed of nanotubes (Figure 1E). Moreover, small tube diameter (30–40 nm) has been demonstrated to accommodate large strain induced by ion insertion.[12] Unlike traditional chemical manganese dioxide (CMD), which tends to form dispersed nanotubes or nanowires, we believe that this hierarchical structure would produce a higher volumetric energy density for battery applications.[13] Meanwhile, from the high-resolution TEM (HRTEM) image (Figure 1F), (111) and (101) facets can be differentiated. The inset fast Fourier transform (FFT) pattern clearly shows (211) and (101) facets. We note that our h-β-MnO_2 is not single-crystalline, in contrast to nanosized β-MnO_2 directly obtained by hydrothermal reaction.[14] To demonstrate the universality of our electrolyte selection criteria, we also included other CMD, α-MnO_2, γ-MnO_2 (Figures S1–S3), and thermally activated commercial EMD powder (Figure S4).

To examine the impact of electrolyte selection on the electrochemical behavior of MnO_2, 1 mol/L $LiPF_6$ in EC: diethyl carbonate (DEC) (50:50 by volume, LP40) was chosen as a common commercial carbonate electrolyte to compare with the aforementioned ether system. Before examining their influence on secondary battery cycling, the primary battery performance was assessed (Figure S5), as electrolyte composition has been demonstrated to have large impact on the first discharge behavior.[15] In doing so, limited difference between carbonate and ether-based electrolytes were observed on the first discharge. At C/20, approximately 250 mAh/g was delivered with a discharge plateau at approximately

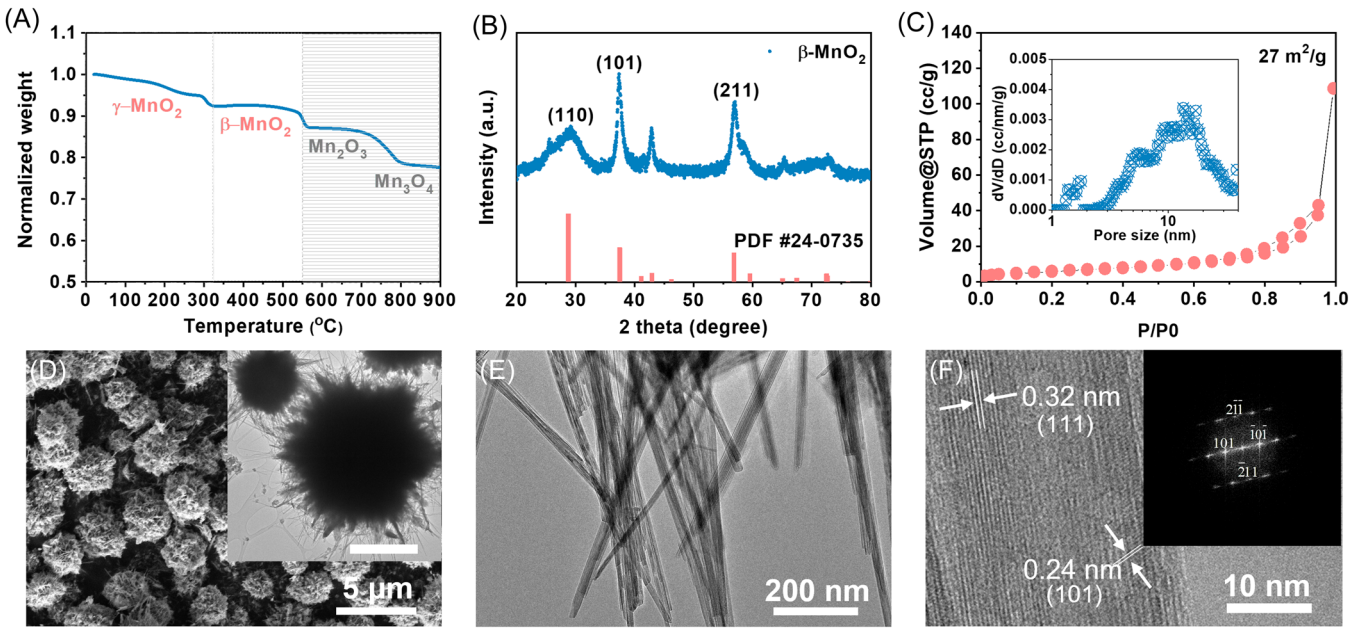

FIGURE 1 (A) TGA of γ-MnO_2 precursor. (B) XRD patterns of h-β-MnO2. (C) N_2 adsorption curves (inset shows pore size distribution). (D) SEM images (inset shows TEM, scale bar is 2 μm). (E) TEM images of the primary structure, and (F) HRTEM images with facets specified (The inset is the FFT of the region from [13-1] direction) of h-β-MnO_2. FFT, fast Fourier transform; HRTEM, high-resolution transmission electron microscope; SEM, scanning electron microscope; TEM, Transmission electron microscopy; TGA, thermogravimetric analysis; XRD, X-ray diffraction.

2.75 V.[7a] When the mass loading was increased over 10 mg/cm^2 (~2.6 mAh/cm^2), negligible capacity drop (Figure S6) was detected.[16] Therefore, it is confirmed that the synthesized h-β-MnO_2 with low crystallinity displays sufficient discharge capacity and output voltage to act as a platform for future study into its rechargeability.

To avoid the parasitic oxidation of ether solvents (Figure S7), the operation window was initially set as 1.8 V–4.0 V. The cycling performance for both electrolytes is exhibited in Figure 2A,B. Though the initial specific capacities were comparable, the capacity loss per cycle between the ether and carbonate systems became distinct during cycling. After 100 cycles, h-β-MnO_2 cycling in ether maintained 144 mAh/g with a 78% capacity retention at C/20, compared to only 69 mAh/g (capacity retention of 38%) in carbonate. When the current density was increased to 1C, the electrode demonstrated 82% capacity retention after 300 cycles in ether, as opposed to 11% in carbonate. Voltage profiles at 1C in Figure 2C,D shows remarkable capacity fading and polarization in carbonate. To consolidate the universal influence of different electrolyte chemistry, other MnO_2 phases were synthesized and applied to long-term cycling (Figure S8), delineated in Figure 2E. Regardless of the phase, the ether electrolyte was found to preserve > 90% capacity retention after 50 cycles, whereas the carbonate system

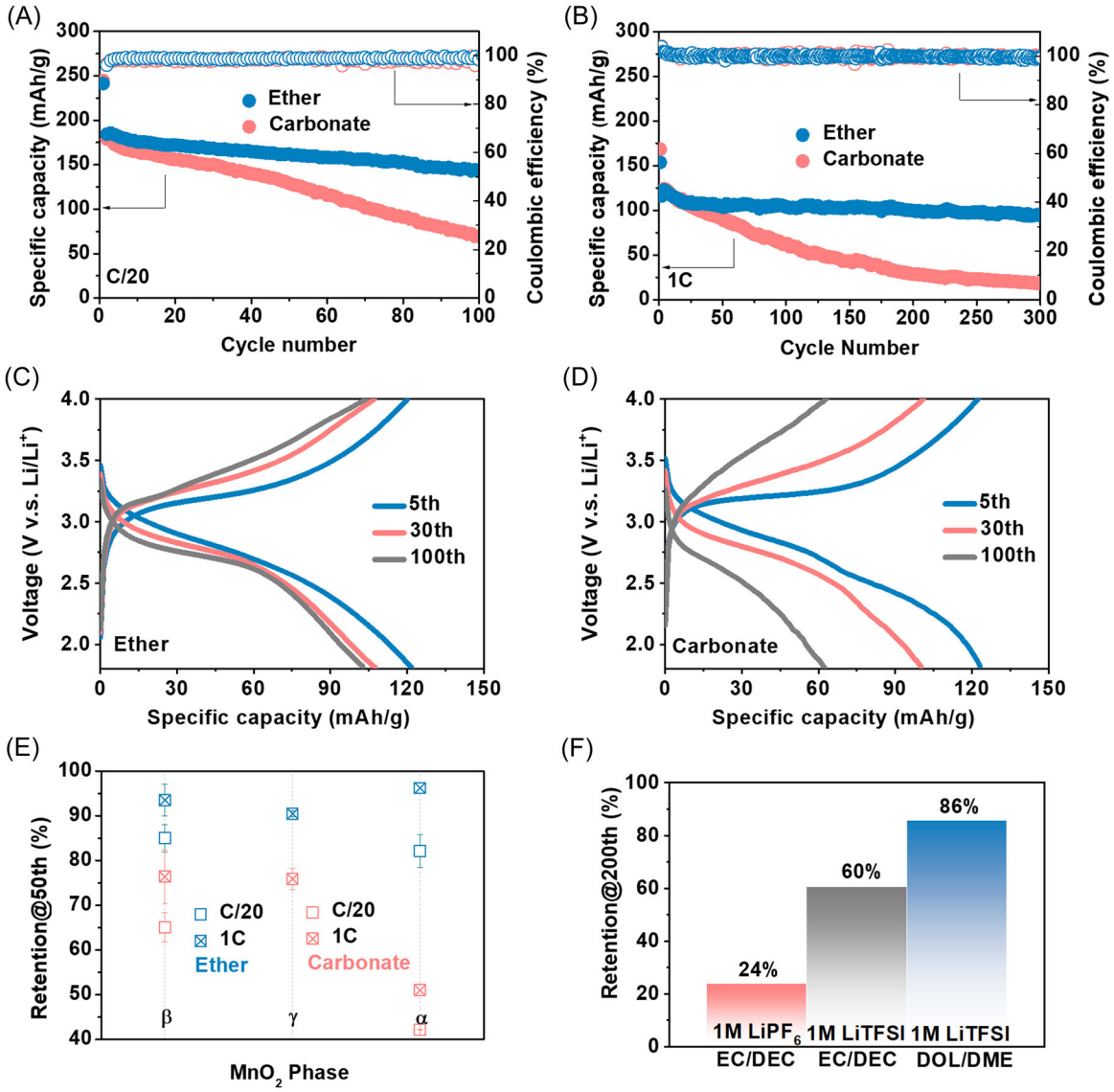

FIGURE 2 Electrochemical performance of h-β-MnO_2 in carbonate, LP40 (1 mol/L $LiPF_6$ EC/DEC) and ether, 1 mol/L LiTFSI DOL/DME at a current density of C/20 (A) and 1C (B). Voltage profiles at 1C in (C) ether, and (D) carbonate. (E) Summary of capacity retention of different CMD with error bar at C/20 and 1C. The generation of error bar is based on at least two repeated cells. (F) Comparison of capacity retention in three electrolytes at 1C using h-β-MnO_2. Discharge capacity is shown. CMD, chemical manganese dioxide; DEC, diethyl carbonate; DOL/DME, 1,3-dioxane/1,2-dimethoxyethane.

produced unstable, highly phase-dependent cycling. Impedance data in Figure S9 reveals that in carbonate, both R_{sei} and R_{ct} were altered considerably, likely due to the increased passivation layer and structure changes on their electrodes.[17] Figures 2F and S10A suggest that the degradation produced by the LP40 system is due to both the solvent and $LiPF_6$, where a LiTFSI in EC/DEC analog produced slightly improved performance relative to LP40, yet less stable than the ether system. Meanwhile, we measured ex-situ XRD (Figure S10B) for cycled h-β-MnO_2 from three electrolytes, where the negligible difference was noticed. These data provide clear evidence that the electrolyte chemistry governs the cyclability of MnO_2 secondary batteries.

The instability of cycled MnO_2 in carbonate is conjectured to be a result from Mn dissolution and accelerated disproportionation reaction of Mn^{3+} in an acidic environment. To provide direct evidence of Mn^{3+} in cycled MnO_2, we employed transmission X-ray microscopy (TXM) with XANES to observe the changes of chemical states of Mn during cycling. Figure 3A suggests that the valence status of Mn is on average is close to 3+ at the discharged state. Figure 3B reflects the spatial distribution of Mn^{3+} at an area scale of approximately 10 μm^2. Only a

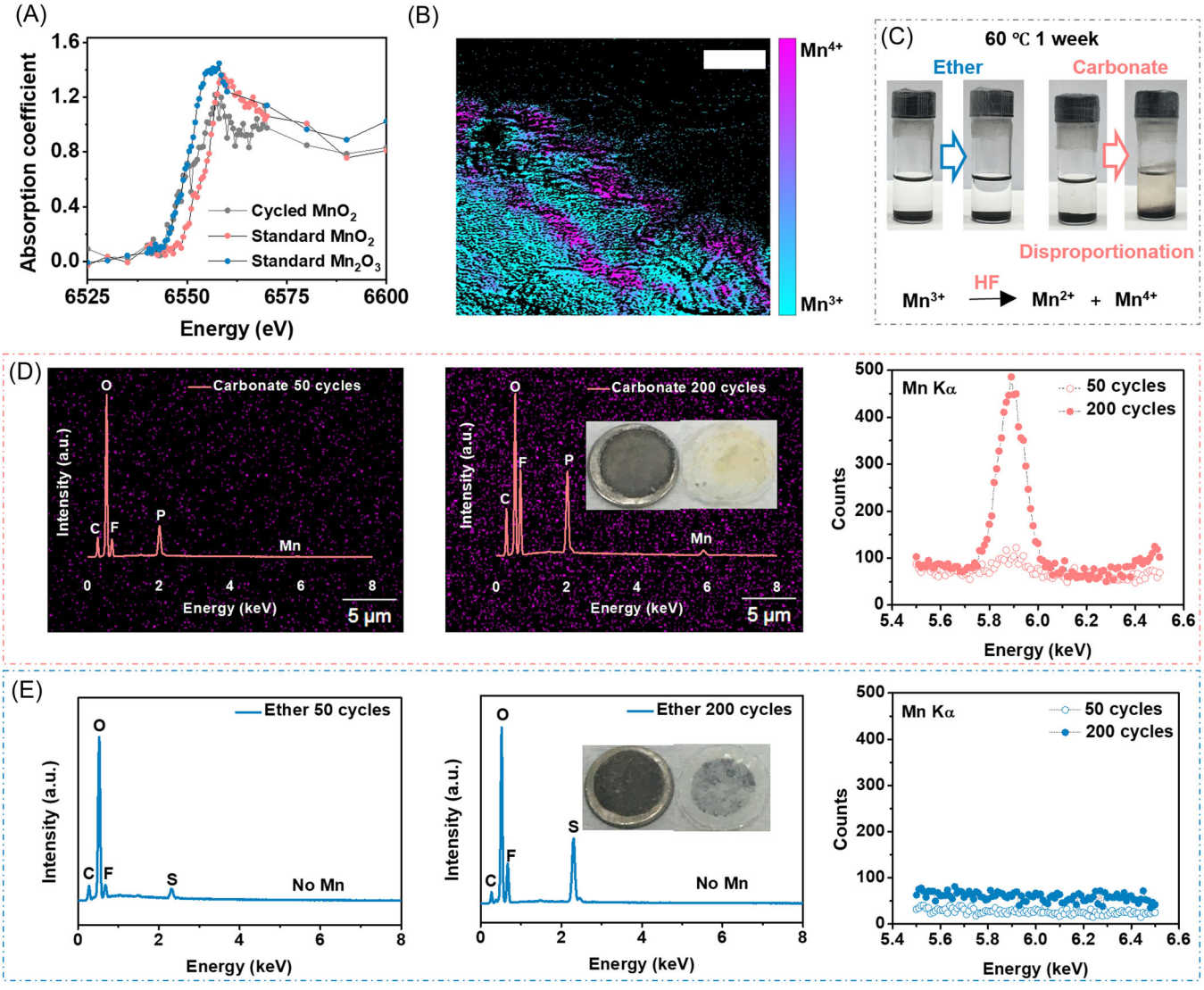

FIGURE 3 (A) X-ray adsorption spectra of different Mn oxides derived from TXM-XANES. (B) Mapping of chemical state for a small part of electrode. MnO_2 is discharged to 1.8 V at C/10 (the first cycle). Scale bar is 1 μm. (C) Photographs of LMO/electrolyte based on ether or carbonate. The arrow points from the image collected at the pristine stage (left) to the image collected after the soak test (right). The sealed vials were heated at 60°C for 1 week. SEM-EDS results of cycled Li after 50 cycles and 200 cycles at 0.5 C in: (D) carbonate (the bottom EDS-Mapping figures clearly shows Mn distribution); (E) ether. The insets in the middle column are photographs of top side of separator and Li metal (facing cathode). Magnification of EDS spectra from 5.5 keV to 6.5 keV is provided at the right column. EDS, energy dispersive X-ray spectroscopy; LMO, $LiMn_2O_4$; SEM, scanning electron microscopy; TXM, transmission X-ray microscopy; XANES, X-ray adsorption near edge spectroscopy.

trace amount of Mn^{4+} is detected, consistent with the high capacity during the first discharge. Abundant Mn^{3+} offers a foundation for studying the effects of different electrolytes. Because pristine MnO_2 is free of Mn^{3+} and the cycled electrodes contain a limited amount of active material, we used $LiMn_2O_4$ powder containing 50% Mn^{3+} in a soak test under elevated temperature. This experiment directly reflects the stability of Mn^{3+} in carbonate and ether (Figure 3C). We observed no change of powder and electrolytes in ether. In contrast, Mn dissolution happens in carbonate. The chemical state of dissolved Mn is reported to be 2+.[18] During electrochemical cycling, dissolved Mn^{2+} can migrate through electrolytes and deposit on Li metal. Therefore, we detached cycled Li-MnO_2 cells and characterized the Li metal anode. As expected, in carbonate, Mn dissolution and deposition process existed more significantly (Figures 3D and S11A,B).[8,19] We also observed a temporal accumulation of Mn on the Li metal. In contrast, no Mn signal was detected with the usage of the ether electrolyte (Figures 3E and S11C,D).

Such difference was also substantiated by other MnO_2 samples such as electrolytic manganese dioxide (EMD), as displayed in Figure S12A–D. It is observed that 1 mol/L LiTFSI EC/DEC also resulted in Mn dissolution (Figure S12E,F), which can explain the notable capacity fading. To summarize, our hypothesis that the ether system without proton generation can resolve Mn dissolution fundamentally in LIBs is supported. More discussion is exhibited in the supplementary discussion and Table S1. At the same time, optical images (insets of Figure 3D,E) manifest that separator in carbonate appeared in a brownish color, a sign of electrolytes decomposition triggered by Mn^{2+}.[20]

We also found that reducing the charging cut-off voltage from 4.0 V to 3.7 V resulted in much-improved cycling stability possibly due to the limited volume expansion and irreversible phase transformation (Figure S13). Therefore, we focused on h-β-MnO_2 being charged to 3.7 V. In terms of cyclability (Figure S14), after 200 cycles, 130 mAh/g and 120 mA/g could be delivered at 0.2 C and 0.5 C, corresponding to capacity retention of 83% and 86%, respectively. β-MnO_2 of 12 h-annealing also demonstrated excellent reversibility (Figure S15) with almost no capacity fading after 300 cycles. All the above data convince that MnO_2 cathode can be highly rechargeable.

To provide a more holistic perspective of the benefits of the ether electrolyte in rechargeable Li-MnO_2 batteries, we apply commercial EMD as the cathode to evaluate cycling stability and the rate performance. At 0.2 C, the EMD presented 130 mAh/g after 200 cycles (96% retention) when applied with the ether electrolyte (Figure 4A). The voltage profile in Figure 4B also reveals that the mid-voltage shows no drop during the cycling

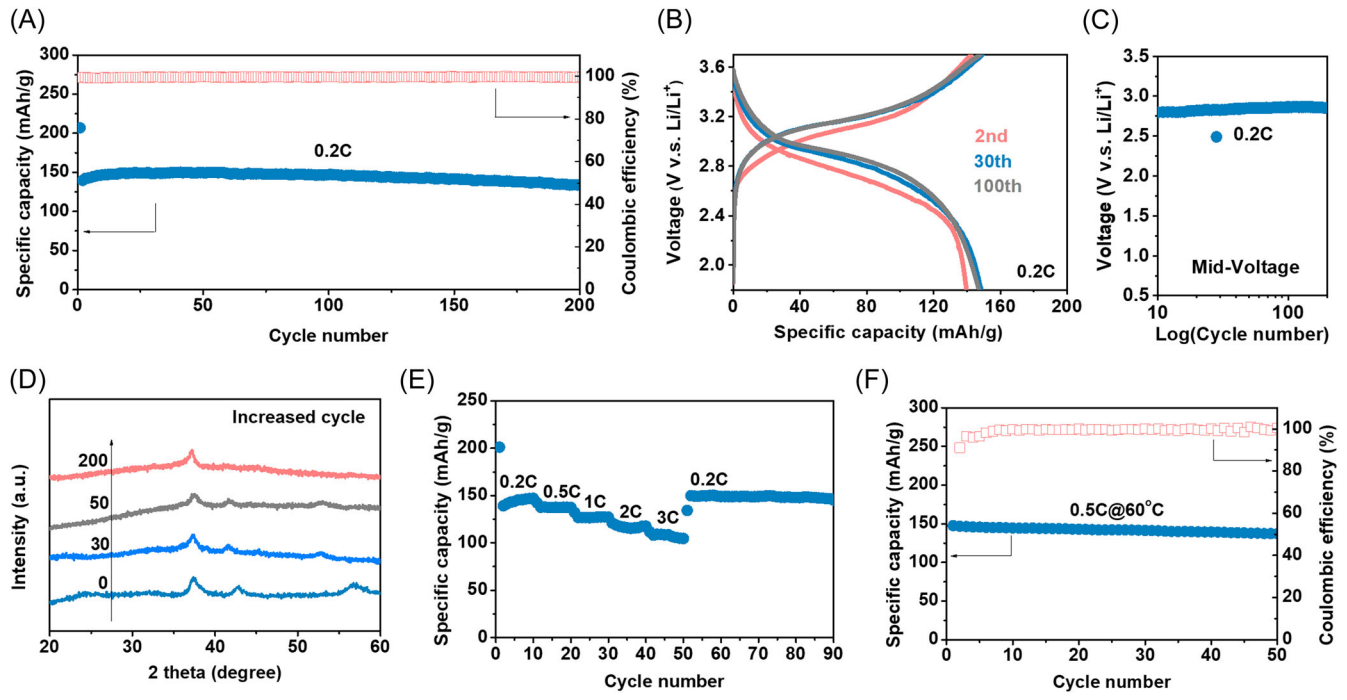

FIGURE 4 Electrochemical performance of activated EMD (EMD heated at 350°C for 12 h) from 1.8 V to 3.7 V: (A) Cycling performance at 0.2 C. (B) Voltage profile at 0.2 C at different cycle numbers. (C) Mid-voltage at 0.2 C. (D) Ex-situ XRD patterns of cycled EMD at 0.5 C at fully charged state at different cycling status. (E) Rate performance from 0.2 C to 3 C. (F) High-temperature cycling at 60°C (0.5 C) with CEs. The first cycle is completed at room temperature. EMD, electrolytic manganese dioxide; XRD, X-ray diffraction.

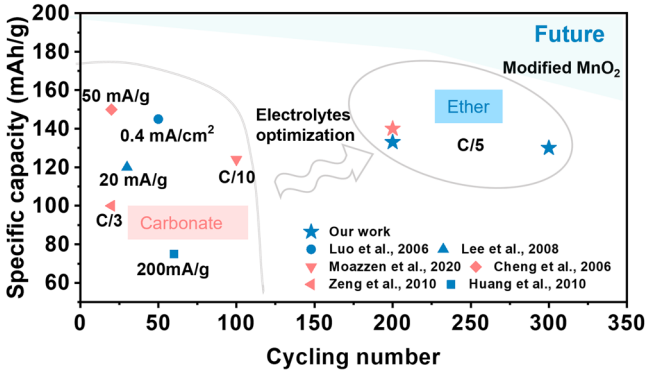

FIGURE 5 Summary of representative cycling data for different MnO_2 cathode compared with our ether-MnO_2 systems. Red and dark cyan color represents γ-MnO_2 and β-MnO_2, respectively. The data points to represent our study are based on Figures 4A, S14A, and S15A. Table S2 presents more information of the prior studies.

process (Figure 4C). Ex-situ XRD reveals minimal irreversible lattice expansion along with amorphization during long cycling occurs (Figures 4D and S16). This can be attributed to the highly disordered spinel-related phase.[21] At 1C, 2C, and 3C, 125 mAh/g, 119 mAh/g, and 110 mAh/g could be output, respectively. Even cycled at 60°C at C/2 (Figure 4F), the EMD cathode still shows a capacity retention of >90% after 50 cycles in the ether electrolyte, suggesting high electrochemical stability.

Therefore, we propose a viable strategy to eliminate Mn dissolution in LIBs based on the application of ether electrolytes, which utilize neither PF_6^- nor EC that has been historically applied in Li-MnO_2 batteries (Table S2). Figures 5 and S18 show our improved cyclability of MnO_2 as well as the promise of the ether electrolyte in Li-MnO_2 cells. In addition, in Figure S19, the cost per kWh for various cathodes were shown. Given the desirable technological maturity in synthesis and modification of MnO_2, there are abundant opportunities for further increasing the cycling life and energy density. For example, $Li_{0.33}MnO_2$ synthesized from EMD by $LiNO_3$ pre-lithiation indicates no dissolution in ether and excellent cyclability (Figure S20).

3 | CONCLUSION

In summary, we demonstrated that common ether electrolytes can repurpose traditional primary Li-MnO_2 batteries to be rechargeable batteries while preserving the low-cost feature. Regardless of the phase or morphology, we found that while Mn dissolution from MnO_2 cathodes is a universal phenomenon with carbonate electrolytes, ether-based electrolytes naturally without proton generation can prevent Mn-based cathodes from dissolution and rapid cell failure. As a result, MnO_2 cathode is exposed to be highly rechargeable as an intercalative cathode. For example, the 1 mol/L LiTFSI DOL/DME (50/50 in volume) ether electrolyte, paired with commercial EMD, was able to deliver a high capacity retention (96%) at 0.2 C for over 200 cycles. In the future, cost-effective MnO_2 as well as further engineered MnO_2 can be more authentically characterized and understood by applying ether electrolytes. Such a simple yet effective strategy toward electrolyte design can pave the way for developing low-cost and more sustainable rechargeable batteries compared with today's LIBs systems.

ACKNOWLEDGMENTS

Z.C. acknowledge the startup fund from the Jacob School of Engineering at UC San Diego. The authors also acknowledge the use of facilities and instrumentation supported by NSF through the UC San Diego Materials Research Science and Engineering Center (UCSD MRSEC) DMR-2011924. Part of the work used the UCSD-MTI Battery Fabrication Facility and the UCSD-Arbin Battery Testing Facility. Electron microscopic characterization was performed at the San Diego Nanotechnology Infrastructure (SDNI) of UCSD, a member of the National Nanotechnology Coordinated Infrastructure, which is supported by the National Science Foundation (Grant ECCS-1542148). Use of the Stanford Synchrotron Radiation Light source, SLAC National Accelerator Laboratory, is supported by the U.S. Department of Energy, Office of Science, Office of Basic Energy Sciences, under Contract No. DE-AC02-76SF00515.

CONFLICT OF INTEREST STATEMENT

The authors declare no conflict of interest.

DATA AVAILABILITY STATEMENT

The data that support the findings of this study are available in the supplementary material of this article.

ORCID

Zheng Chen http://orcid.org/0000-0002-9186-4298

REFERENCES

1. Dühnen S, Betz J, Kolek M, Schmuch R, Winter M, Placke T. Toward green battery cells: perspective on materials and technologies. *Small Methods*. 2020;4(7):2000039.
2. a Li M, Lu J. Cobalt in lithium-ion batteries. *Science*. 2020;367(6487):979-980; b Xu P, Tan DHS, Chen Z. Emerging trends in sustainable battery chemistries. *Trends Chem*. 2021;3(8):620-630.
3. Johnson CS. Development and utility of manganese oxides as cathodes in lithium batteries. *J Power Sources*. 2007;165(2): 559-565.

4. Blomgren GE. The development and future of lithium ion batteries. *J Electrochem Soc*. 2016;164(1):A5019-A5025.
5. Luo J-Y, Zhang J-J, Xia Y-Y. Highly electrochemical reaction of lithium in the ordered mesoporosus β-MnO_2. *Chem Mater*. 2006;18(23):5618-5623.
6. a Asl HY, Manthiram A. Reining in dissolved transition-metal ions. *Science*. 2020;369(6500):140-141; b Yu Y, Karayaylali P, et al. Coupled $LiPF_6$ decomposition and carbonate dehydrogenation enhanced by highly covalent metal oxides in high-energy Li-ion batteries. *J Phys Chem C*. 2018;122(48):27368-27382.
7. a Ren Y, Armstrong AR, Jiao F, Bruce PG. Influence of size on the rate of mesoporous electrodes for lithium batteries. *J Am Chem Soc*. 2010;132(3):996-1004; b Jiao F, Bruce PG. Mesoporous crystalline β-MnO_2—a reversible positive electrode for rechargeable lithium batteries. *Advanced Materials*. 2007;19(5):657-660.
8. Zhan C, Wu T, Lu J, Amine K. Dissolution, migration, and deposition of transition metal ions in Li-ion batteries exemplified by mn-based cathodes-a critical review. *Energy Environ Sci*. 2018;11(2):243-257.
9. a Cho Y-G, Jung S-H, Joo SH, et al. A metal-ion-chelating organogel electrolyte for le chatelier depression of Mn^{3+} disproportionation of lithium manganese oxide spinel. *J Mater Chem A*. 2018;6(45):22483-22488; b Ryou M-H, Hong S, Winter M, Lee H, Choi JW. Improved cycle lives of $LiMn_2O_4$ cathodes in lithium ion batteries by an alginate biopolymer from seaweed. *J Mater Chem A*. 2013;1(48):15224-15229; c Yang X, Li J, Xing L, Liao Y., Xu M., Huang Q., Li W. Stabilizing lithium manganese oxide/organic carbonate electrolyte interface with a simple boron-containing additive. *Electrochimica Acta*. 2017;227:24-32.
10. a Yuan Y, Liu C, Byles BW, et al. Ordering heterogeneity of [MnO_6] octahedra in tunnel-structured MnO_2 and its influence on ion storage. *Joule*. 2019;3(2):471-484; b Dose WM, Donne SW. Kinetic analysis of γ-MnO_2 thermal treatment. *J Thermal Anal Calorimetry*. 2011;105(1):113-122.
11. Dose WM, Sharma N, Webster NAS, Peterson VK, Donne SW. Kinetics of the thermally-induced structural rearrangement of γ-MnO_2. *J Phys Chem C*. 2014;118(42):24257-24265.
12. Sayle TXT, Maphanga RR, Ngoepe PE, Sayle DC. Predicting the electrochemical properties of MnO_2 nanomaterials used in rechargeable li batteries: simulating nanostructure at the atomistic level. *J Am Chem Soc*. 2009;131(17):6161-6173.
13. Wang D, Liu H, Li M, et al. Nanosheet-assembled hierarchical $Li_4Ti_5O_{12}$ microspheres for high-volumetric-density and high-rate Li-ion battery anode. *Energy Storage Mater*. 2019;21:361-371.
14. Wang X, Li Y. Synthesis and formation mechanism of manganese dioxide nanowires/nanorods. *Chem - A Eur J*. 2003;9(1):300-306.
15. Takahashi M, Yoshimura S, Nakane I, et al. A study on electrolytes for manganese dioxide-lithium cells. *J Power Sources*. 1993;43(1):253-258.
16. Wang L, Wu Z, Zou J, et al. Li-free cathode materials for high energy density lithium batteries. *Joule*. 2019;3(9):2086-2102.
17. Zhan C, Lu J, Jeremy Kropf A, et al. Mn(II) deposition on anodes and its effects on capacity fade in spinel lithium manganate–carbon systems. *Nat Commun*. 2013;4(1):2437.
18. Zhou G, Sun X, Li Q-H, et al. Mn ion dissolution mechanism for lithium-ion battery with $LiMn_2O_4$ cathode: in situ ultraviolet–visible spectroscopy and ab initio molecular dynamics simulations. *J Phys Chem Lett*. 2020;11(8):3051-3057.
19. Shin J, Seo JK, Yaylian R, Huang A, Meng YS. A review on mechanistic understanding of MnO2 in aqueous electrolyte for electrical energy storage systems. *Int Mater Rev*. 2020;65(6):356-387.
20. Wang C, Xing L, Vatamanu J, et al. Overlooked electrolyte destabilization by manganese (II) in lithium-ion batteries. *Nat Commun*. 2019;10(1):3423.
21. Tan H, Wang S, Lei X. New insights for the cyclic performance of Li/MnO_2 batteries using a simple electrochemical process. *J Electrochem Soc*. 2015;162(3):A448-A452.

SUPPORTING INFORMATION

Additional supporting information can be found online in the Supporting Information section at the end of this article.

How to cite this article: Xia D, Gao H, Li M, et al. Enabling rechargeable Li-MnO_2 batteries using ether electrolytes. *SmartMat*. 2023;e1208. doi:10.1002/smm2.1208